Original Article

Seismic hazard prediction using multispectral amplification maps in a complex topographic area: A case study of Qiaozhuang town, Sichuan Province, Southwest China

LUO Yong-hong[1]* https://orcid.org/0000-0001-7462-1182; e-mail: lyh445890689@qq.com

XU Qiang[1] https://orcid.org/0000-0001-5894-4694; e-mail: xq@cdut.edu.cn

ZHAN Wei-wei[2] https://orcid.org/0000-0002-9266-4466; e-mail: weiwei.zhan@tufts.edu

GRELLE Gerardo[3]* https://orcid.org/0000-0002-7820-5896; e-mail: gerardo.grelle @uniroma1.it

Corresponding author

1 State Key Laboratory of Geo-Hazard Prevention and Geo-Environment Protection, Chengdu University of Technology, Chengdu 610059, China

2 Department of Civil and Environmental Engineering, Tufts University, Medford, MA 02155, USA

3 Department of Civil and Environment Engineering, University of Rome, Rome 00184, Italy

Abstract: Earthquakes can cause widely distributed slope failures and damage in mountainous areas. The accurate prediction of ground motions in mountainous areas is essential for managing the seismic risk of urban cities near mountains but is restricted primarily by complex seismic site amplification effects in areas of uneven terrain. This study selected Qiaozhuang town located in the Qingchuan−Pingwu fault zone, Southwest China, as a case study. A simulator for mapped seismic responses using a hybrid model (SiSeRHMap) was applied to compute the multispectral seismic topographic amplification maps at the three slope units surrounding Qiaozhuang town (Weigan hill, Mt. Dong, and Mt. Shizi). Post-earthquake damage survey maps, 1D seismic site response spectral ratios, and *H/V* spectral ratios of earthquake data were used to validate the computed seismic site amplification factors and resonance frequencies. The results suggest that strong topographic amplification effects usually occur at distinct slope locations, such as hilltops, convex slope positions, upslope, and narrow ridges. The computed topographic amplification factors in the study area reached up to 2.4 at upslope or hilltops, and the resonance frequencies were between 3 and 10 Hz. Topographic effects can be as important as stratigraphic effects when assessing seismic amplification effects in the study area. We conclude that both topographic and stratigraphic effects should be considered in the comprehensive seismic hazard assessment of the study area or other similar mountain towns.

Keywords: Seismic hazard prediction; Multispectral amplification map; topographic effects; Stratigraphic effects; SiSeRHMap; Wenchuan earthquake.

1 Introduction

Strong earthquakes can cause widely distributed

geological hazards in mountainous areas, leading to heavy casualties and property losses. For example, as of September 25, 2008, the Wenchuan earthquake had killed 69,227 people in total, with 17,923 people missing (Tao and Tao 2021), and one-third of the total casualties were caused by slope failures (Huang and Li 2008). Assessing the site seismic responses of slopes is an essential component for the accurate prediction of ground motions in hilly/mountainous areas. Site seismic responses are affected by various factors, such as topography (Griffiths and Bollinger 1979), stratigraphy (Luo et al. 2021), rock structures/ faults (Martino et al. 2006; Gischig et al. 2015), groundwater (Huang et al. 2016) and seismic wave types (Semblat et al. 2000).

Topographic effects on seismic ground motions have been extensively studied in the last few decades. These studies have investigated the effects of different factors on topographic site effects, such as canyon topography (Wong and Jennings 1975; Chiu and Huang 1992; Sepúlveda et al. 2005), surface curvature (Maufroy et al. 2015; Torgoev and Havenith 2016), local topography (Hough et al. 2010) and slope angle (Di Fiore 2010). Some studies have integrated stratigraphic effects with topographic effects to explain strong seismic amplifications (Chuhan and Chongbin 1988; Luo et al. 2020; Grelle et al. 2021).

Topographic site effects are frequency-dependent 3D seismic amplification phenomena (Lawrence and Lewis 1973; Celebi 1991; Maufroy et al. 2015). The peak amplification at the slope crest occurs at a normalized frequency of $H/\lambda= 0.2$, where H is the slope height and λ is the wavelength of the motion (Scott et al. 1997). The observed seismic site amplification factors at slopes can vary by a factor of up to 10 for frequencies between 1 and 10 Hz (Aki 1993; Faccioli 1991). Analyses of seismic recordings in the Santa Monica Mountains indicate an amplification at a predominant frequency of $f=V/4h$ (V is the layer velocity and h is the layer thickness) at $f \sim 3.6$ Hz for S-waves and $f \sim 7.9$ Hz for P-waves (Graizer. 2009). Seismic slope instability and dynamic slope deformation analyses are also frequency-dependent (Jafarzadeh et al. 2015).

To predict site seismic effects over large areas, simplified GIS software packages have been developed in recent years (Maufroy et al. 2012; Rai et al. 2016; Grelle et al. 2016; Wang et al. 2018). For instance, the simulator for mapped seismic response using a hybrid model (SiSeRHMap) is a GIS-based

approach developed by Grelle et al. (2016) that can compute combined topographic and stratigraphic effects over large areas. SiSeRHMap has been applied to several case studies in different regions, such as the East Mountain and Port au Prince (Haiti) regions (Grelle et al. 2018) and the Red Zone sector of Amatrice hill (Grelle et al. 2020).

This study aims to improve the seismic hazard management for a mountain town by assessing the site seismic effects of slopes surrounding the town with the aid of the GIS-based approach, SiSeRHMap. We chose Qiaozhuang town in Qingchuan County as the study area, which is located in Sichuan Province, Southwest China. According to postearthquake surveys, the 2008 Ms 8.0 Wenchuan earthquake induced strong seismic site amplification effects on the slopes in the study area where slope cracks and rockfalls were widely distributed along the ridge (Luo et al. 2014). Analyses of aftershock recordings revealed that the resonance frequencies were 2 to 5 Hz at the hilltop and up to 7 Hz downslope of Weigan hill, located on the southern edge of the study area (Luo et al. 2014). Ambient noise analyses suggested that Weigan hill has a low resonance frequency (~1 Hz), while Mt. Dong and Mt. Shizi have intermediate and high resonance frequencies (~4 Hz and 7~20 Hz, respectively) (Del Gaudio et al. 2018). Shallow seismic reflection and geological surveys revealed the geological structure in the study area (Luo et al. 2021). Computationally expensive discrete element analyses revealed that both topographic and stratigraphic effects significantly impact the slope seismic amplification phenomena in the study area (Luo et al. 2020). This study further evaluates the effectiveness of a simplified GIS-based site response approach (SiSeRHMap) in the study area. The findings of this work will also be insightful for regional seismic hazard assessments in other mountainous areas.

2　Geological and Geomorphological Settings

This work selected Qiaozhuang town, located in the Qingchuan–Pingwu (QC–PW) fault zone (Fig. 1). Three branches of the QC–PW fault pass through the northern part of Qiaozhuang town and dip steeply towards the northwest. The 2008 Ms 8.0 Wenchuan earthquake caused severe damage in Qiaozhuang town. After the main shock of the Wenchuan earthquake, more than 2000 aftershocks with a
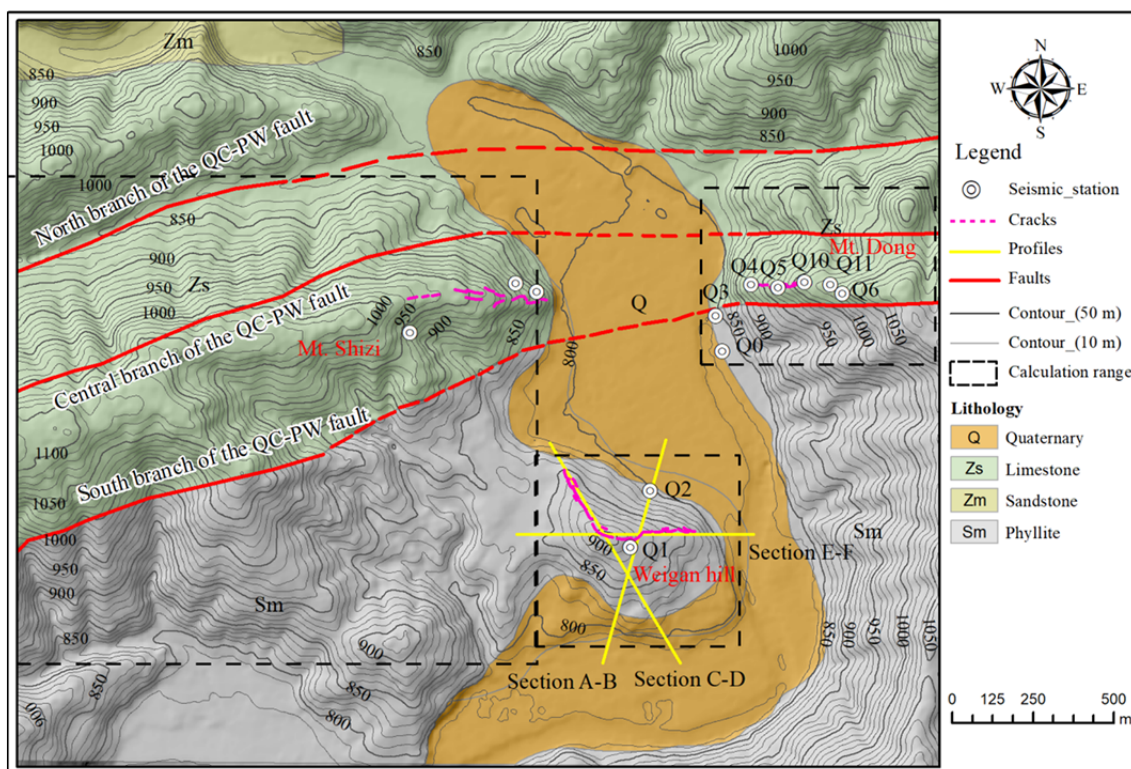
Fig. 1 Geological sketch map of the area surrounding Qiaozhuang town in Qingchuan County (modified after Luo et al. 2020). Three sections were used to analyse the microtopography amplification: A-B has a NE-SW orientation, C-D has a NW-SE orientation, and E-F has an E-W orientation.

maximum Ms of 6.0 occurred around the study area (Liu et al. 2009), and the aftershock nearest the study area was approximately 4 km away. The study area is situated at altitudes between 780 and 1200 m and includes several landforms, such as terraces, hills, and low mountains. Qiaozhuang town sits on Quaternary alluvial sediment deposited within the valley. Weigan hill is a small hill located near the southern edge of Qiaozhuang town and consists of two ridges: the west ridge with a strike of N30°W and the east ridge with a strike of N90°E. Two seismic monitoring stations, Q1 and Q2, were installed near the hilltop and toe of Weigan hill to monitor the aftershock activities, respectively. Mt. Dong is located on the east side of Qiaozhuang town and consists of several thin ridges and valleys. The seismic array at Mt. Dong includes five seismic stations along the ridge (from top to bottom: Q6, Q11, Q10, Q5, and Q4) and two seismic stations at the slope toe (Q3 and Q0). The third slope unit investigated in this work, Mt. Shizi, is located on the west side of Qiaozhuang town and is a thick ridge with a strike close to N90°E. Weigan hill consists of phyllite with dense schistosity, while Mts. Dong and Shizi are composed mainly of limestone. The P-wave velocity of the overburden ranges from 724 to 1024

m/s, the limestone is characterized by a mean velocity of 1470 m/s to 3760 m/s, and the phyllite is characterized by a mean velocity of 1440 m/s to 3580 m/s (Luo et al. 2021).

3 Data and Methods

To obtain the seismic response maps across the study area characterized by uneven terrain and shallow sediment cover, we employed the simulator for mapped seismic response using a hybrid model (SiSeRHMap) developed by Grelle et al. (2016). SiSeRHMap is a computer program capable of generating maps of predicted seismic site responses considering stratigraphic and topographic effects. This methodology is implemented using the Python programming language and is available at https://www.geosmartapp.it. SiSeRHMap consists of five sequential modules (Fig. 2). Module 0 is the preprocessing module for gathering lithostratigraphic information. Module 1 parameterizes the relationship between the shear-wave velocity (Vs) and depth (z). Module 2 builds a 3D subsoil model (called the GIS cubic model (GCM)) using available and randomized
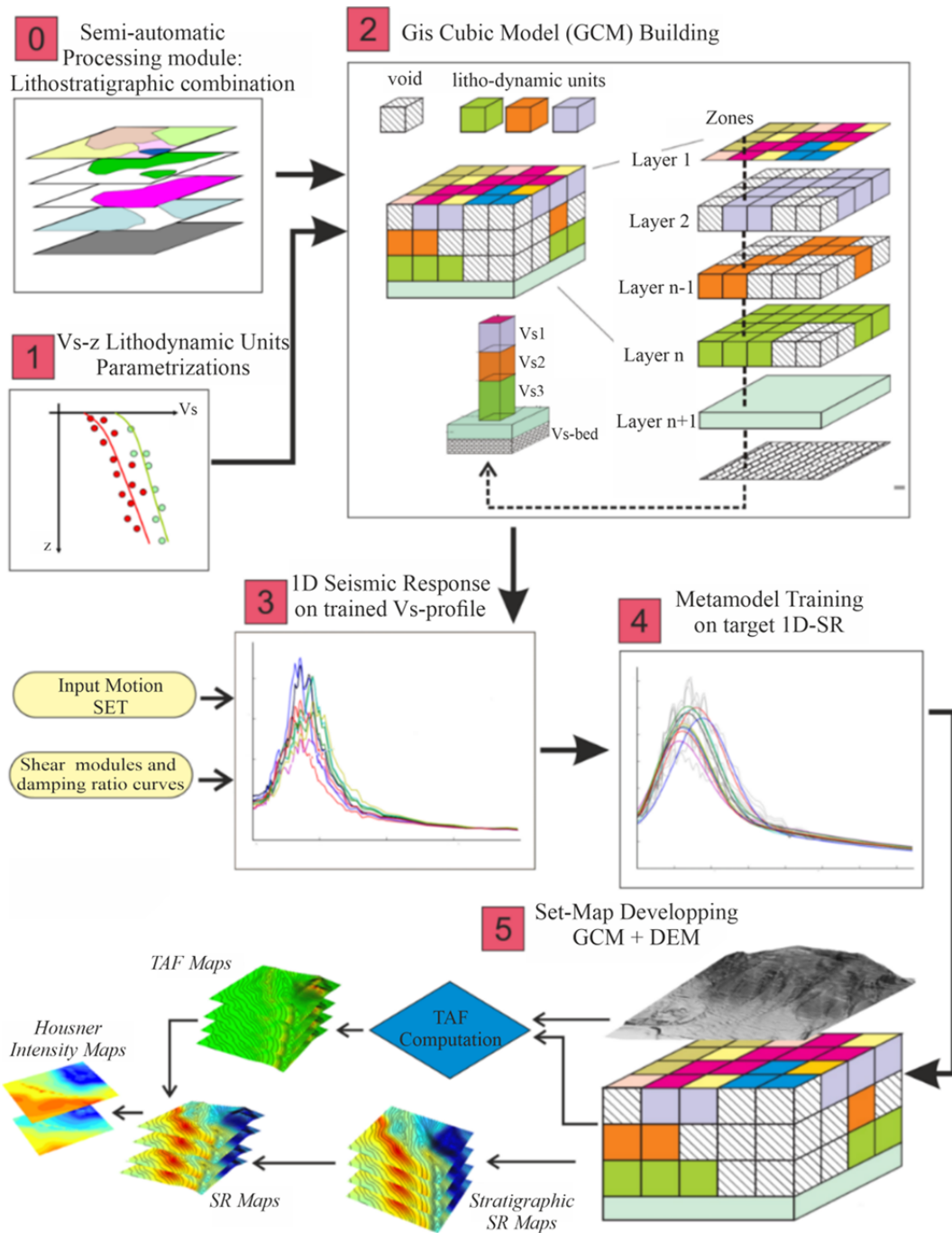
Fig. 2 Flowchart of the SiSeRHMap computational methodology (Grelle et al. 2020).

Vs profiles and geometry information. Module 3 predicts the acceleration response spectra using a 1D seismic response analysis based on the equivalent linear approach. Module 4 trains a surrogate model (called a metamodel) to predict the acceleration response spectra at discrete periods using independent variables, such as the average Vs of near-surface lithodynamic units, the elastic fundamental period of the soil sequence (T_f), and the period of

interest. Finally, Module 5 generates hybrid seismic response maps integrating (1) stratigraphic seismic responses computed using the metamodel derived in Module 4 with (2) topographic aggravation factors (TAFs) computed using an empirical TAF function that is dependent on the morphometric shape and equivalent uniform shear-wave velocity of the topographic materials (Grelle et al. 2020).

The minimum resolutions of the raster input data

for the stratigraphic and topographic responses are suggested to be 10 and 30 m, respectively. More details about this methodology are available in Grelle et al. (2016, 2020). Some key components and required data of this methodology used in this study are described as follows. Considering the aim of this work and the coupled hybrid treatment of stratigraphic and topographic effects in SiSeRHMap, we computed the seismic responses by
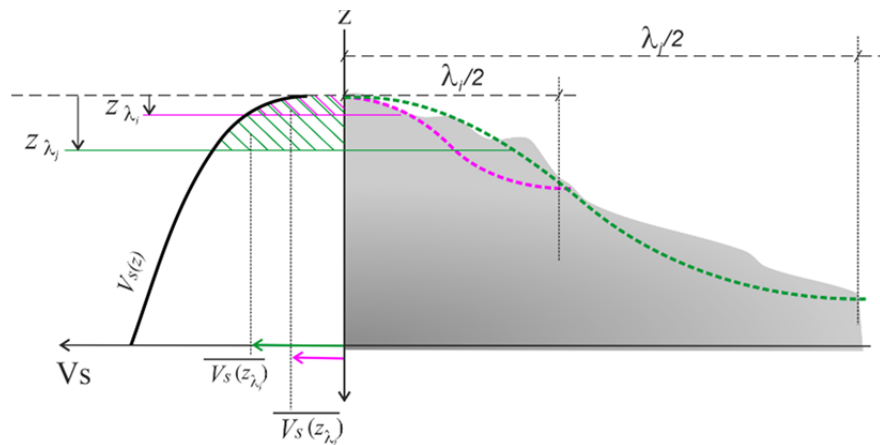

Fig. 3 Computational model for nonuniform topographic relief: the left side shows the $Vs(z)$ distribution and the z_λ sectors identified by enveloping wavelengths, and the right side shows the two generic wavelengths enveloping the topographic surface.

considering the topographic effect of the complete extensive relief (digital elevation map (DEM) data) and 1D stratigraphic responses at some relevant monitoring sites. These results are marked in Fig. 1 as Q1 and Q2 for Weigan hill and Q4, Q5, Q6, Q10, and Q11 for Mt. Dong, and the subsoil Vs sequences of the sectors in which they are located are well known. Thus, in this phase, computational modules were not used to develop maps of the 1D seismic responses. Instead, a more simplified approach of using SiSeRHMap to process single Vs profiles at the monitoring sites was performed. The computation of a map requires the whole area to be well characterized, but the requisite amount of subsoil data needed to meet this requirement in the study area have not yet been obtained. Hence, geological and geophysical surveys will be performed in future works.

This work provides the opportunity to control the evolution of the topographic module, as well as the possibility of considering nonuniform relief. Such tasks are aimed at compliance between the natural increase in Vs with depth and the stratigraphic Vs profile considered in the 1D stratigraphic analysis. According to Grelle et al. 2016, this condition can be defined by the following general relationship:

$$Vs(z) = Vs_0 + \alpha \ln(z) \tag{1}$$

where Vs_0 is the intercept of the shear-wave velocity (>0 but can be usually or unrealistically low for soil materials) and α is the log-linear gradient. Therefore, the extension model (Fig. 3) considers that different relevant z_λ sectors are affected by enveloping wavelengths, λ; thus, each period (frequency) of vibration is assumed to define the TAF function. In

this regard, the Vs of each sector is computed as the integral mean solution solved according to the variable z as follows:

$$\overline{Vs(z)} = \frac{1}{z}\int_0^z Vs_0 + \alpha \, ln(z). \tag{2}$$

The z_i value defines the sector as substantially enveloped by the ith wavelength, and it is computed in relation to the spatial resolution of the map, $L_{(x,y)}$, which is initially defined as the standard input of 30 m in SiSeRHMap, and the extension parameter of the enveloping wave. These formulas include the wave frequency and shear-wave velocity of the ridge sector over z_i.

$$z_{\lambda i} = \frac{1}{4}\left(L_{(x,y)} + \frac{\overline{Vs(z_{i-1})}}{2f}\right) \tag{3}$$

The above equation is progressively computed to resolve Eq. 2 by initially assuming that for i=0, z_0=0. This condition is identified by the peak ground acceleration (PGA) condition $\lambda \to 0$, $f \to \infty$. Therefore, the enveloping wavelengths generated by high frequencies define all sectors with values of approximately $L_{(x,y)/4}$ (=7.5 m, considering the initial standard resolution of 30 m). In this way, considering $\overline{Vs(z_{i-1})} = Vs_0$, relevant values of z_λ (that increase the initial value) are produced with Eq. 3 starting from f=10 Hz. This frequency is usually assumed to be the first value of the TAF spectral series, while Vs_0 is an unreal velocity.

Table 1 lists the input uniform Vs values used to compute the TAFs for the three slope units within the study area (i.e., Weigan hill, Mt. Dong, and Mt. Shizi). Table 2 shows the characteristic stratigraphic profiles at the monitoring stations at Weigan hill and Mt. Dong used for the 1D seismic response analysis.

Table 1 Shear-wave velocities (SWV(m/s)) of the Quaternary deposit and bedrock layers at the three slope units in the study area.

Location	Layer	SWV	Remarks
Weigan hill	Deposit	345	Block stone and gravel soil
	Bedrock	695	Weathered bedrock
Mt. Dong	Deposit	349	Block stone and gravel soil
	Bedrock	709	Weathered bedrock
Mt. Shizi	Deposit	330	Block stone and gravel soil
	Bedrock	732	Weathered bedrock

In the nonuniform topographic model, the TAFs were computed by considering the vertical Vs profile trends (Eq. 1). The $Vs-z$ regression parameters, Vs_0 and α were determined to be 23 m/s and 230, respectively, for Weigan hill and 1 m/s and 336 for Mt. Dong. In this way, the model defines different

responses by successively considering the stiffness ($\overline{Vs(z)}$) of each of the z sectors (Eq. 2) affected by the enveloping wavelengths and considering each frequency of vibration assumed to define the spectral TAF function. To demonstrate this, Fig. 4 shows the relation between the above mentioned parameters considered in the nonuniform topographic analysis of Weigan hill.

The topographic amplification function relies on several topographic parameters, such as curvature, slope and elevation. We obtained these parameters by processing a digital terrain model (DTM) with a spatial resolution of 30 m. This resolution represents half of the minimum wavelength and was used as the topographic source data for the SiSeRHMap computation. Regarding the stratigraphic

Table 2 Geological material properties for the 1D seismic site response analyses

| Number	Geological features	Mean thickness (m)	Density (kg/m³)	Shear-wave velocity (m/s)	Damping* D_0 (%)	Remarks
Layer 1	Phyllite with strong surface weathering	15	2150	345.0	2.0	
Layer 2	Phyllite with strong to medium weathering	18	2200	695.0	1.0	
Layer 3	Phyllite with medium to weak weathering	23	2300	1207.2	0.5	Weigan hill
Layer 4	Phyllite with weak weathering to hard phyllite	23	2350	1653.5	0.5	(Q1 and Q2)
Layer 5	Hard phyllite	>100	2500	2008.9	0.5	
Layer 1	Dolomite with strong surface weathering	10	2000	342.6	2.0	
Layer 2	Dolomite with strong to medium weathering	20	2200	727.0	1.0	Mt. Dong
Layer 3	Dolomite with medium to weak weathering	10	2400	1233.0	0.5	(Q4, Q5, Q6,
Layer 4	Dolomite with weak weathering to hard Dolomite	25	2500	1683.0	0.5	Q10 and
Layer 5	Hard Dolomite	>100	2600	2886.0	0.5	Q11)
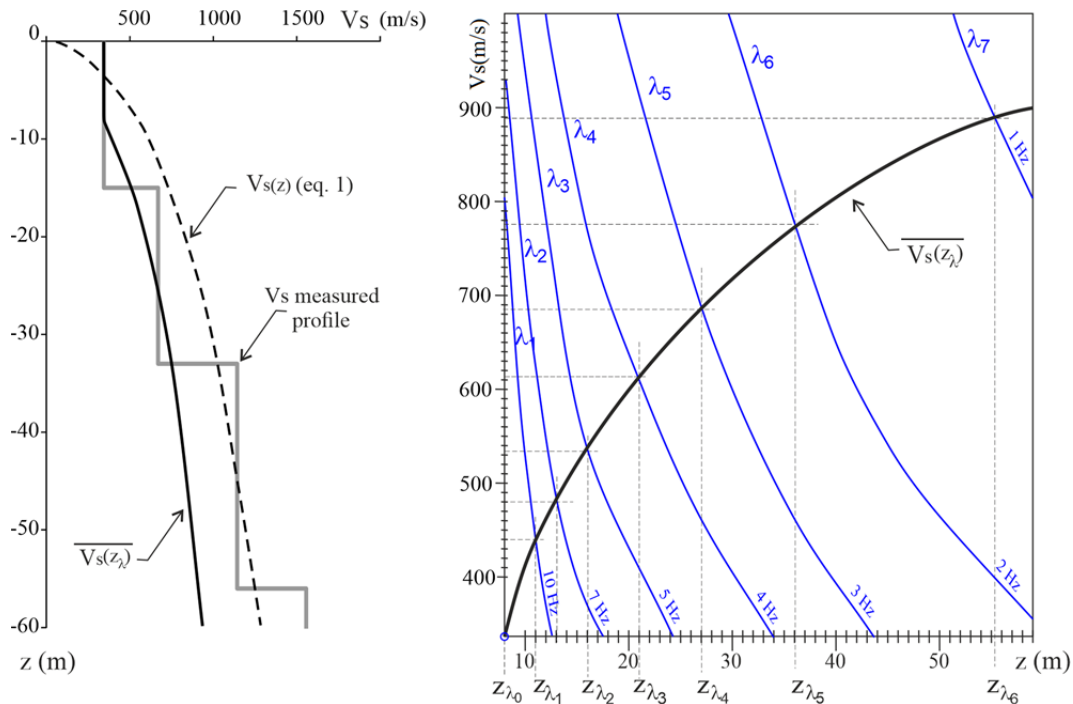
Fig. 4 Example of a discretized z_λ sector for Weigan hill.

amplification effects, a strongly weathered lithology was applied in the computation. The *Vs* values derived from geophysical investigations (Luo et al. 2021) and used in Module 5 (Fig. 2) are listed in Table 1.

Additionally, based on aftershock recordings and ambient noise analysis in the study area (Luo et al. 2014, 2020; Del Gaudio et al. 2018), we generated a set of maps showing the TAFs at a set of discrete frequencies (i.e., 1, 2, 3, 4, 5, 7, 10, and 100 Hz) for the three slope units in the study area. We validated our modelling results using multiple sources of observation data, such as slope damage maps from postearthquake surveys, H/V spectral ratios of aftershocks, and 1D site response analysis results at representative seismic stations. These comparisons permitted an evaluation of the reliability of the SiSeRHMap approach for the prediction of seismic

hazards in complex topographic environments.

4 Results

4.1 Weigan hill

Fig. 5 shows maps of the TAFs at varying frequencies at Weigan hill derived from the two uniform *Vs* models. The hilltop and upslope (TAF= 2.2~2.4) show more substantial topographic amplification effects than the downslope and terrace (TAF= 1.0~1.5) regardless of the *Vs* used in the uniform model. The input uniform *Vs* influences the amplitude of the TAF, frequencies, and locations of the strongest topographic effects. When the input uniform *Vs* is 345 m/s (see Fig. 5a), the strongest TAF appears at the upslope section for the intermediate
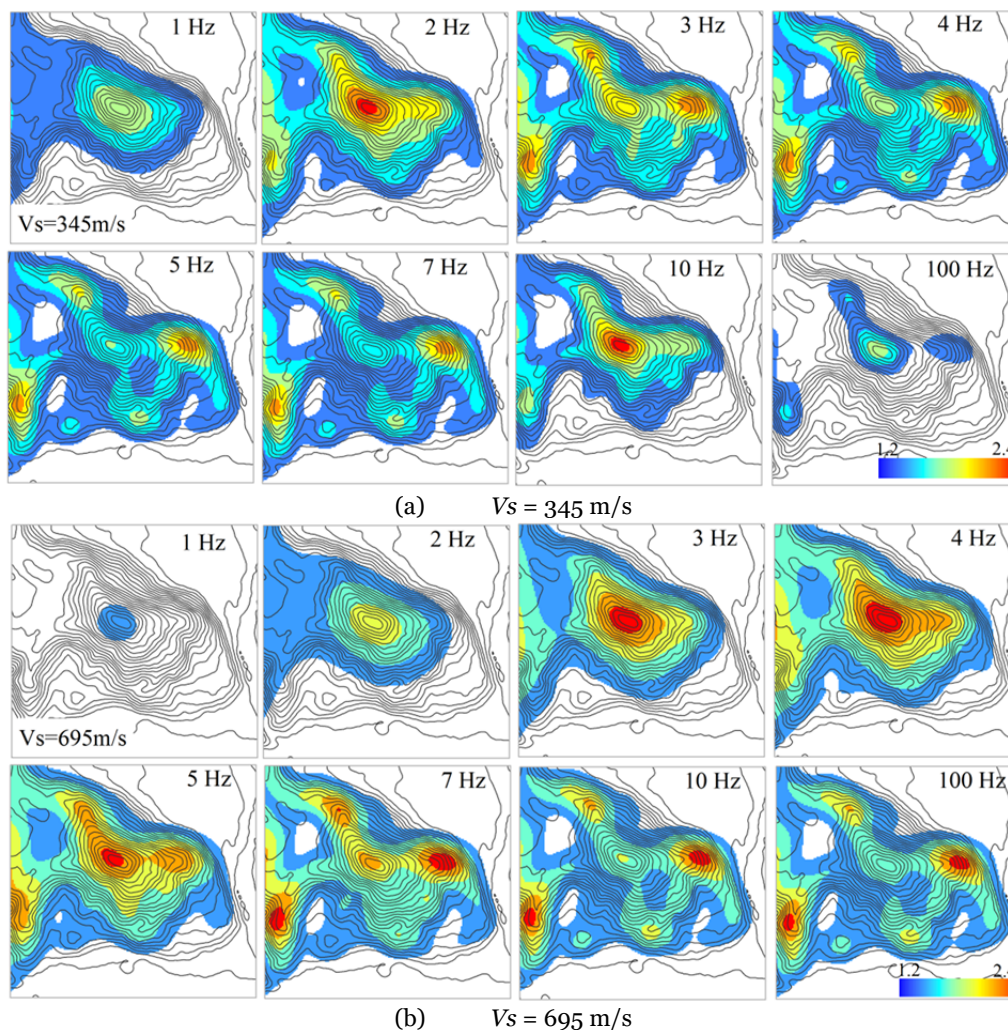

Fig. 5 Maps of the topographic aggravation factors (TAFs) at Weigan hill computed with a uniform *Vs* model: (a) *Vs* = 345 m/s and (b) *Vs* = 695 m/s.

frequencies (i.e., 3, 4, 5, and 7 Hz) and at the hilltop for both low (1 and 2 Hz) and high frequencies (10 and 100 Hz). When the input uniform *Vs* is 695 m/s (see Fig. 5b), the strongest TAF appears at the hilltop for frequencies less than 5 Hz and upslope for frequencies larger than 7 Hz. Comparing the TAFs across frequencies at the top of Weigan hill, we found that strong topographic amplification occurs at 2 and 10 Hz and at 3~5 Hz when the input uniform *Vs* is 345 and 695 m/s, respectively. At several upslope sections of Weigan hill, large TAFs appear at intermediate frequencies (i.e., 3, 4, 5, and 7 Hz) when the input uniform *Vs* is 345 m/s and at high frequencies (7, 10, 100 Hz) when the input uniform *Vs* is 695 m/s.

Fig. 6 displays maps of the TAFs at Weigan hill derived from the nonuniform *Vs* model accounting for both stratigraphic and topographic effects. The computed TAFs of the nonuniform *Vs* model show a similar spatial distribution pattern. Strong topographic amplification appears along the ridge, where more substantial amplification occurs at the hilltop for intermediate frequencies (i.e., 2, 3, and 4 Hz) and upslope for high frequencies (i.e., 5, 7, 10, and 100 Hz). The spatial distribution of seismic cracks across Weigan hill induced by the Ms 8.0 Wenchuan earthquake matches well with the TAF maps for high frequencies, especially 5~100 Hz. As the high-frequency ground motion components are strongly correlated with the PGA, ground motions along the ridge may have high PGAs due to strong site amplification.

We further investigated the microtopographic effects at Weigan hill by plotting the frequency-dependent TAFs along three representative section profiles (see Fig. 7): a section along the west ridge (C-D), a section along the east ridge (E-F), and a section perpendicular to the main strike of Weigan hill (A-B) (the locations of these three sections are marked in Fig. 1). The strongest TAFs occur at the hilltop and the convex position of the slope (i.e., the transition position between the gentle upslope and the steeper downslope) and have amplitudes between 1.8 and 2.4 (Fig. 7). The strongest TAFs at the convex position of the east ridge (Fig. 7a) are slightly larger than those at the convex position of the west ridge (Fig. 7b), which implies that the microtopographic slope curvature may influence the topographic amplification effects. In addition, the input *Vs* models influence the resonance frequencies (see Fig. 7), which suggests that both the topography and the stratigraphy can influence the seismic amplification effects on uneven terrain in a coupled way.

4.2 Mt. Dong and Mt. Shizi

Mt. Dong and Mt. Shizi produced earthquake damage during the Wenchuan main shock. Fig. 8 shows the TAFs at Mt. Dong computed using the nonuniform Vs model with Vs values of 349 m/s and 709 m/s for the deposit and bedrock layers, respectively. The results suggest that the ground motions are severely amplified along the mountain ridge, especially at high frequencies. Strong TAFs
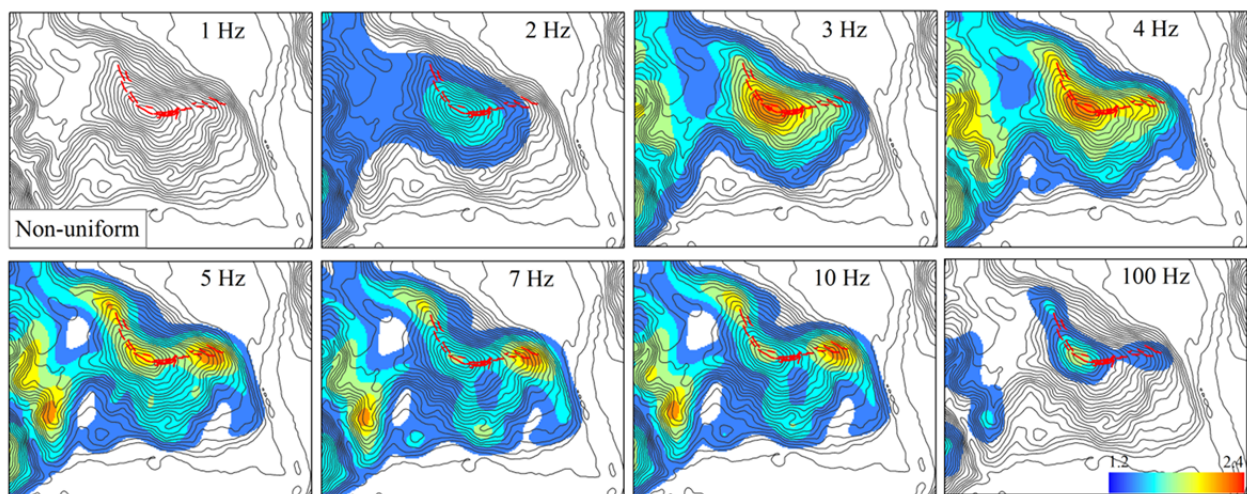

Fig. 6 Maps of the topographic aggravation factors (TAFs) at Weigan hill computed with a nonuniform *Vs* model that consists of a surface deposit layer (*Vs* = 345 m/s) and a bedrock layer (*Vs* = 695 m/s). The red lines indicate the mapped seismic cracks induced by the 2008 Ms 8.0 Wenchuan earthquake.
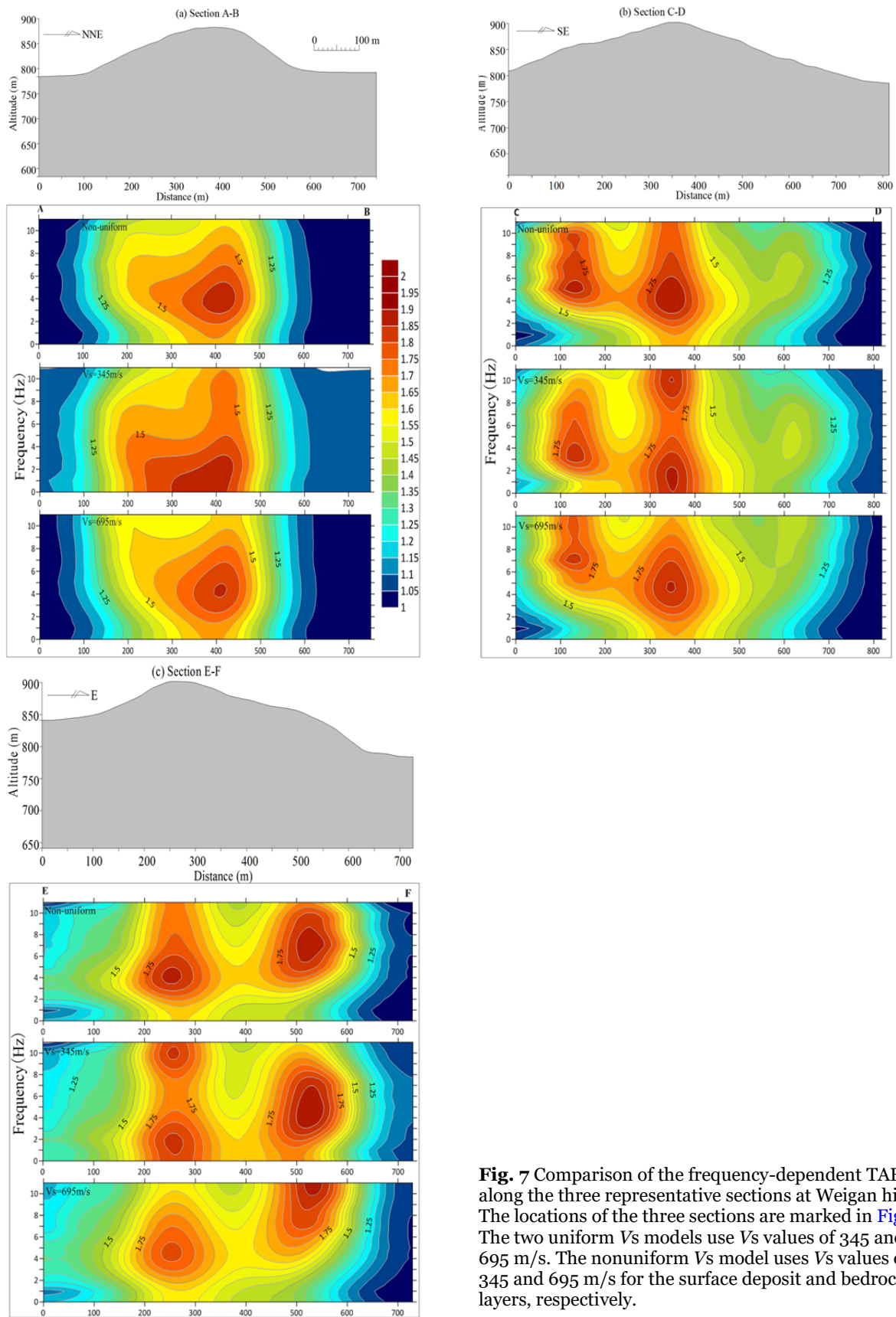
Fig. 7 Comparison of the frequency-dependent TAFs along the three representative sections at Weigan hill. The locations of the three sections are marked in Fig. 1. The two uniform *V*s models use *V*s values of 345 and 695 m/s. The nonuniform *V*s model uses *V*s values of 345 and 695 m/s for the surface deposit and bedrock layers, respectively.
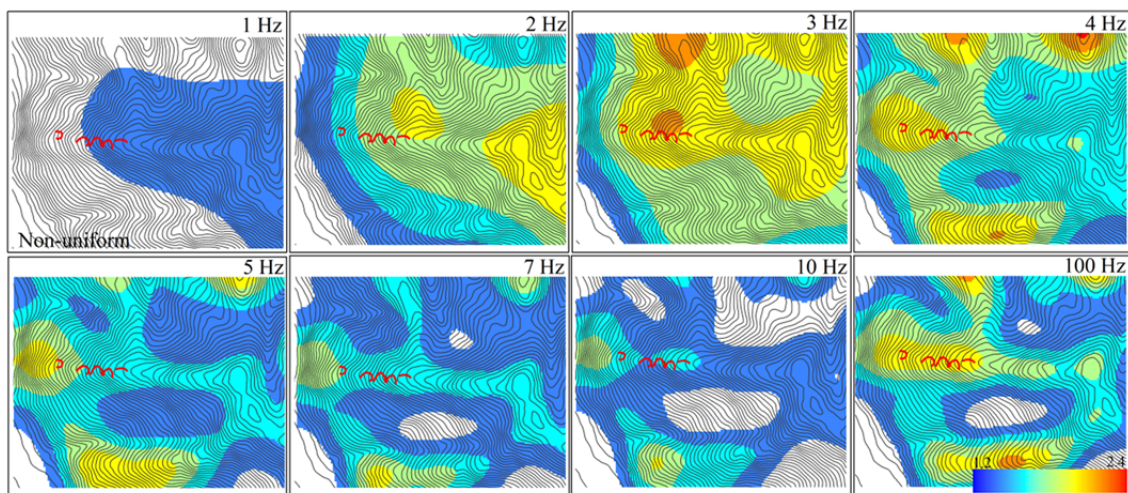
Fig. 8 Maps of the topographic aggravation factors (TAFs) at Mt. Dong computed with a nonuniform *Vs* model that consists of a surface deposit layer (*Vs* = 349 m/s) and a bedrock layer (*Vs* = 709 m/s). The red lines indicate the mapped seismic cracks induced by the 2008 Ms 8.0 Wenchuan earthquake.

appear to occur at locations characterized by microtopographic features, such as the convex positions of slopes, narrow ridges, and slope break positions. The TAFs are mainly in the range of 1.5~2.0, and the largest TAF is approximately 2.4. The spatial distribution of seismic cracks at Mt. Dong induced by the Wenchuan earthquake (Xu et al. 2009a) is spatially consistent with the zones of strong topographic amplification effects.

Fig. 9 shows the TAFs at Mt. Shizi computed using the nonuniform Vs model with Vs values of 330 m/s and 732 m/s for the deposit and bedrock layers, respectively. The microtopographic features, such as the upslope, narrow ridge, hilltop and slope convex positions, show strong topographic amplification effects, which is similar to the results at Mt. Dong.

The seismic cracks at Mt. Shizi induced by the Wenchuan earthquake are located in the downslope section of the main ridge, which is consistent with the predicted strong seismic amplification zones (see the upper right corner in Fig. 9). Other strong seismic amplification zones at Mt. Shizi do not have in situ damage survey data (Xu et al. 2009b), which prevents a complete comparison in this area.

5   Discussion

The study area is characterized by high seismic risk. It is therefore important to discuss seismic risk mitigation strategies for the study area based on the computational site amplification results and the existing elements at risk. Although most residential buildings in the study area are located within the valley, several temples and scenic overlook platforms are built at the top of Weigan hill, and some residential buildings are located on the three slope units (i.e., Weigan hill, Mt Dong, and Mt. Shizi). Our computational results show that the TAFs are high along the ridge, especially at the hilltop and the convex positions of the slope; the resonance frequencies are 3~4 Hz and 5~10 Hz at the hilltop and upslope, respectively. Thus, future building designs in these areas should avoid the construction of buildings with a similar natural vibration frequency, and seismic mitigation measures should be conducted to reduce the seismic risk of the existing buildings. According to the empirical correlation between the natural vibration period and building height ($T=(0.05\sim0.075)H^{3/4}$, where H is the height and T is the natural vibration period of the building) (GB50011-2010), building structures with heights of 1.5~12 m (approximately 1 to 4 stories) are at high seismic risk corresponding to resonance frequencies of 3 to 10 Hz. In addition, the severe seismic amplification effects along the ridge can cause secondary geological hazards such as rockfalls and landslides, which can imperil the people and properties at the slope and valley. Future studies can further investigate the comprehensive seismic risk of Qiaozhuang town by considering seismic site amplification effects and subsequent slope failures.

Our analyses have shown that the topographic amplification maps are generally consistent with the spatial distribution of mapped seismic damage.We further examined the SiSeRHMap methodology by
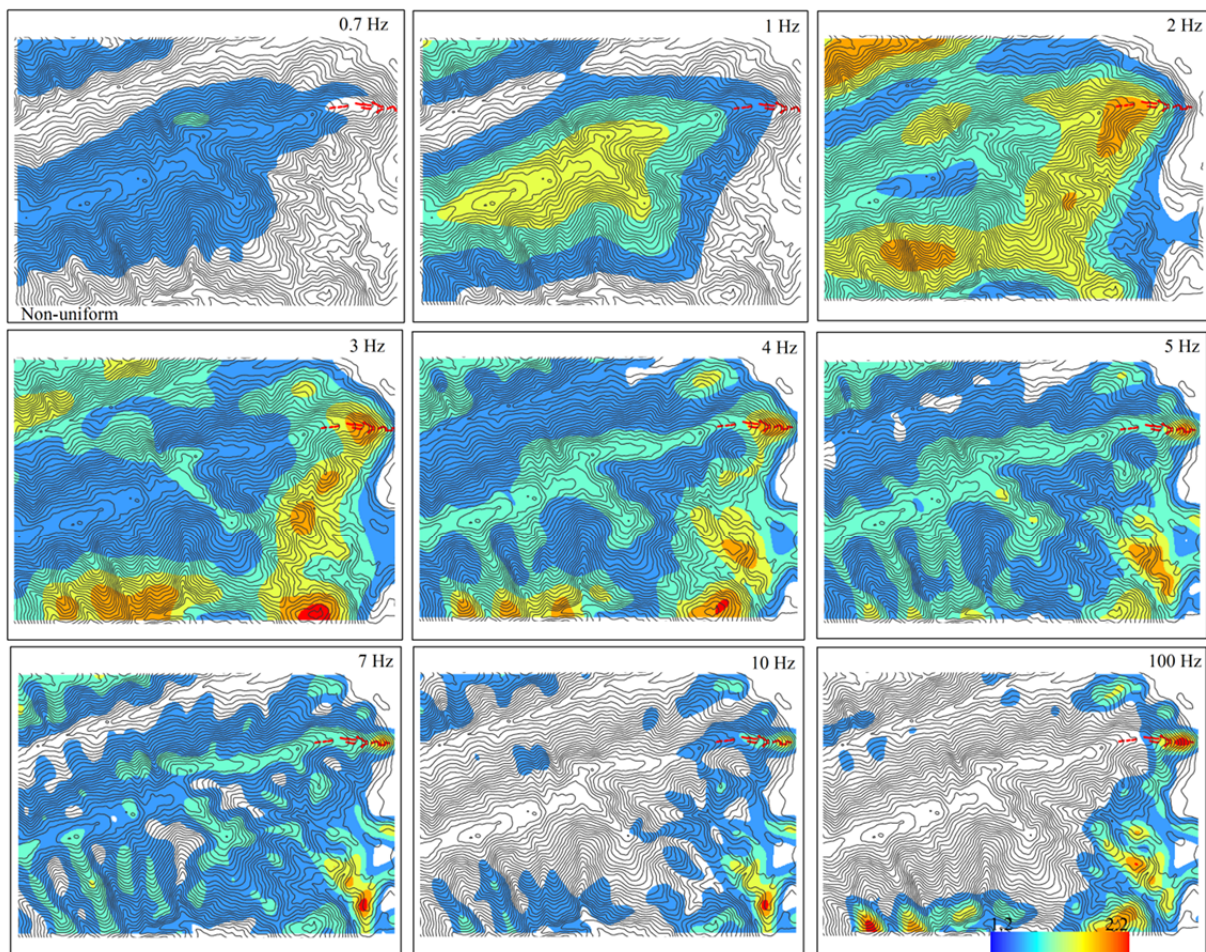
Fig. 9 Maps of the topographic aggravation factors (TAFs) at Mt. Shizi computed with a nonuniform Vs model that consists of a surface deposit layer (Vs = 330 m/s) and a bedrock layer (*Vs* = 732 m/s). The red lines indicate the mapped seismic cracks induced by the 2008 Ms 8.0 Wenchuan earthquake.

comparing the spectral ratio curves derived from 1D seismic site response analyses and *H/V* spectral ratio curves derived from weak ground motion analyses. 1D SH propagation model of SiSeRHMap (Grelle et al. 2016) was assumed to meet the weak seismic motions. We considered the uncertainty in the 1D site response analysis due to the uncertain *Vs* profile data. The mean characterizations of the stratigraphic profiles at the seismic monitoring stations are listed in Table 2. We used the Monte Carlo technique to develop n.30 *Vs* profile assuming ±15% variability of the input mean parameters (*Vs* and thickness). The mean results and standard deviations from the 1D seismic site response analyses were compared with the TAFs derived from the SiSeRHMap analyses using the nonuniform *Vs* model (Fig. 10). In the monitoring sites, TAF curve peaks well accord in frequency with the 1D spectral ratio ones; around 3Hz for Weigan hill and 2 to 4.5Hz for Mt Dong (Fig. 10). This effect can

explain the severity of the vibration involving the monitoring sites and so in producing the rock-failure phenomena. In addition, the coupled stratigraphic and topographic effects well match the H/V ratio in terms of the amplification frequency and amplitude (Fig. 11).

At Weigan hill, the peak frequencies of our SiSeRHMap analyses at stations Q1 and Q2 match the first and second peak frequencies of the corresponding *H/V* ratio curves, respectively. However, a peak frequency (~5 Hz) observed in the *H/V* spectral ratio curve at Q1 is not captured by SiSeRHMap analyses. We suggest that this is likely caused by the simplified two-layer structure of the nonuniform Vs model for the SiSeRHMap analyses that may overlook some details of the stratigraphic sequence (e.g., fractured-weak layer). At Mt. Dong, the *H/V* spectral ratios match well with the computed spectral ratios for the downslope stations (Q4, Q5,
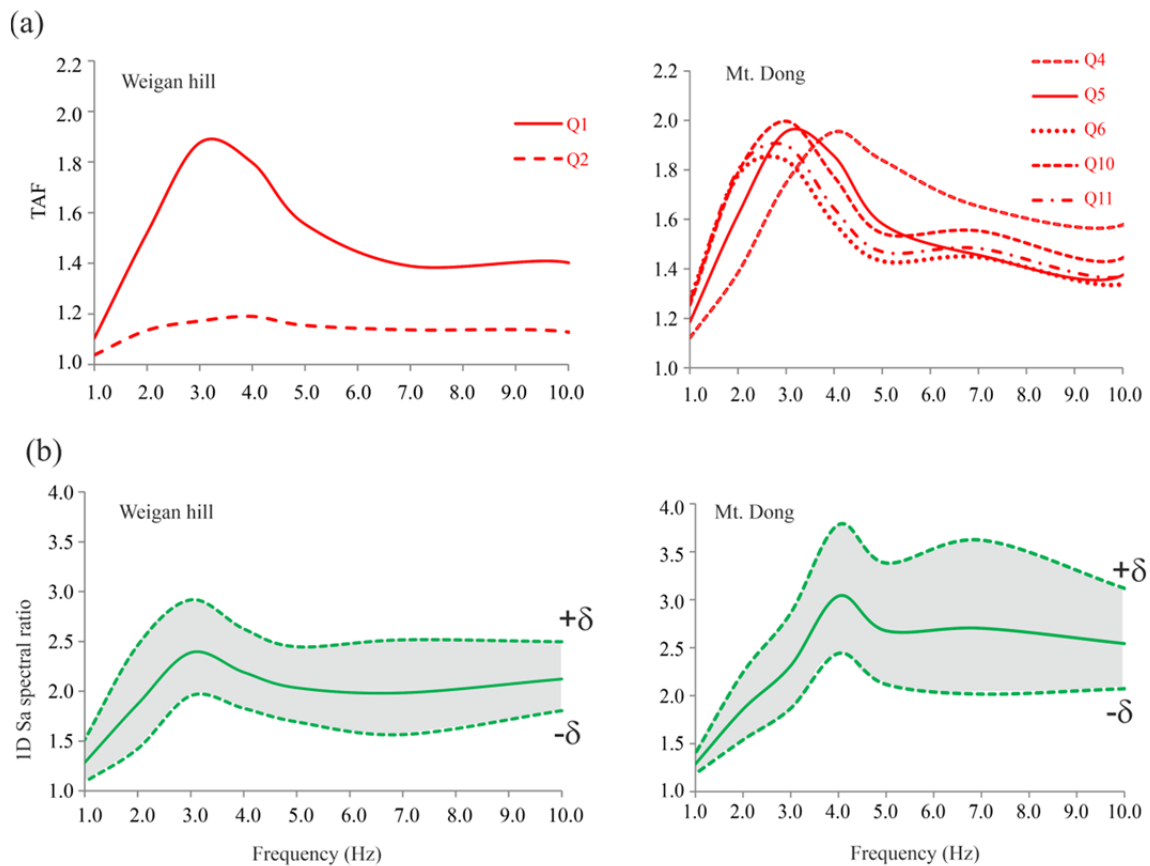
Fig. 10 Comparison of the topographic and stratigraphic effects at the seismic monitoring stations at Weigan hill and Mt. Dong: (a) TAF curves extracted from the SiSeRHMap analyses using the non-uniform model and (b) 1D spectral ratio curves computed using the 1D seismic site response analyses assuming variable input parameters (δ is the standard deviation).
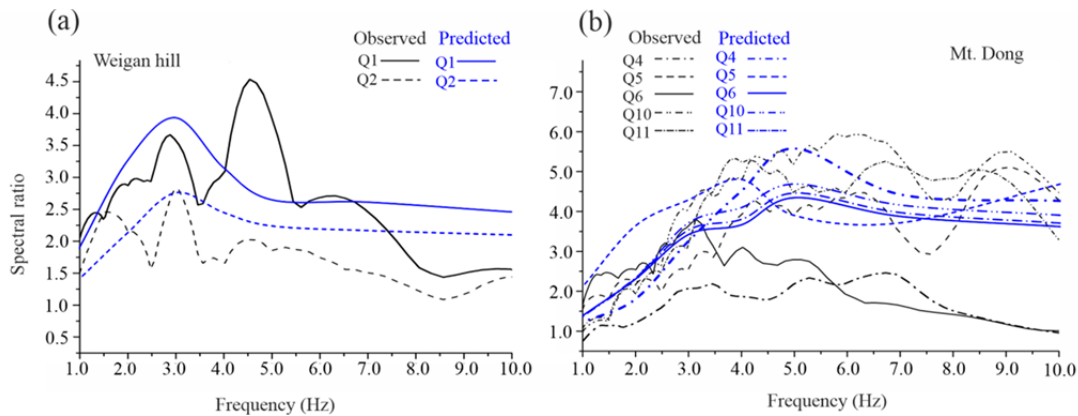

Fig. 11 Comparison of the spectral ratios predicted using SiSeRHMap (blue lines) with the observed H/V spectral ratios (black lines) deriving from the weak ground motions (revised from Luo et al. 2020) recorded at the seismic monitoring stations: (a) Weigan hill and (b) Mt. Dong.

and Q10), while the *H/V* spectral ratios at the upslope stations (Q6 and Q10) show lower resonance frequencies and amplitudes than the computed spectral ratios. The uneven distribution of soft surface deposits along the slope may cause this issue, as the upslope deposit is usually thinner than the downslope deposit. Nevertheless, the SiSeRHMap methodology shows a reasonable prediction of seismic amplification effects in our study area. Its ability to generate seismic amplification maps using a GIS-based methodology will benefit seismic hazard assessment across large mountainous areas.

6 Conclusion

In this paper, we deployed the SiSeRHMap methodology to study the seismic amplification effects at three slope units (Weigan hill, Mt. Dong, and Mt. Shizi) surrounding Qiaozhuang town, Qingchuan County, Southwest China. The computed results are compared with multiple sources of data, such as postearthquake damage survey data, *H/V* spectral ratios from earthquake recordings, and 1D seismic site response analyses considering input parameter uncertainties. The results highlight the combined role of topographic and stratigraphic effects in seismic site response analyses in areas of uneven terrain covered by soft Quaternary deposits or unevenly weathered bedrock. The main conclusions include the following:

(1) The topographic amplification maps computed using the SiSeRHMap methodology are generally consistent with the spatial distribution of seismic cracks induced by the 2008 Ms 8.0 Wenchuan earthquake at the three slope units.

(2) Strong topographic amplification effects usually occur at distinct slope locations, such as hilltops, convex slope positions, upslope, and narrow ridges.

(3) The computed amplification effects are influenced by multiple factors, such as the surface *Vs* structure and slope geometry. The TAFs and resonance frequencies vary at different slope locations. The computed TAFs in the study area reach up to 2.4. The resonance frequencies are between 3 to 10 Hz.

(4) The coupled effects of topography and stratigraphy have important meaning for seismic amplification effect assessments in the study area. The spectral ratios predicted using nonuniform *Vs* model (SiSeRHMap) and observed analyses at monitoring sites show similar amplitudes and close resonance frequencies.

In summary, this work demonstrates that the GIS-based SiSeRHMap approach can be reasonably used to predict seismic amplification effects in uneven terrain. Future studies will need to improve the comprehensive seismic hazard assessment methodology by improving the characterization of the geological structure in the study area and considering types of secondary geological hazards.

Acknowledgements

References

Aki K (1993) Local site effects on weak and strong ground motion. Tectonophysics 218(1-3):93-111. https://doi.org/10.1016/0040-1951(93)90262-I

Celebi M (1991) Topographical and geological amplification: case studies and engineering implications. Struct Saf 10(1-3):199-217. https://doi.org/10.1016/0167-4730(91)90015-2

Chiu HC, Huang HC (1992) Effects of the canyon topography on ground motions at the Feitsui damsite. Bull Seismol Soc Am 82(4):1646-1660. https://doi.org/10.1785/BSSA0820041646

Chuhan Z, Chongbin Z (1988) Effects of canyon topography and geological conditions on strong ground motion. Earthq Eng Struc Dyn 16(1): 81-97. https://doi.org/10.1016/0148-9062(88)91488-x

Del Gaudio V, Luo Y, Wang Y, et al. (2018) Using ambient noise to characterise seismic slope response: the case of Qiaozhuang peri-urban hillslopes (Sichuan, China). Eng Geol 246: 374-390. https://doi.org/10.1016/j.enggeo.2018.10.008

Di Fiore V(2010) Seismic site amplification induced by topographic irregularity: Results of a numerical analysis on 2D synthetic models. Eng Geol 114(3-4): 109-115. https://doi.org/10.1016/j.enggeo.2010.05.006

Faccioli E(1991) Seismic amplification in the presence of geological and topographic irregularities. Inte Conferences on Recent Advances in Geotechnical Earthquake Engineering and Soil Dynamics 2:1779-1797. https://scholarsmine.mst.edu/icrageesd/02icrageesd/session14/13

Griffiths DW, Bollinger GA (1979) The effect of Appalachian Mountain topography on seismic waves. Bull Seismol Soc Am 69(4): 1081-1105 https://doi.org/10.1785/BSSA0690041081

Gischig VS, Eberhardt E, Moore JR, et al. (2015) On the seismic response of deep-seated rock slope instabilities—Insights from numerical modeling. Eng Geol 193:1-18. https://doi.org/10.1016/j.enggeo.2015.04.003

Graizer V (2009) Low-velocity zone and topography as a source of site amplification effect on Tarzana hill, California. Soil Dyn Earthq Eng 29(2): 324-332. https://doi.org/10.1016/j.soildyn.2008.03.005

Grelle G, Bonito L, Lampasi A, et al. (2016) SiSeRHMap v1. 0: a simulator for mapped seismic response using a hybrid

model. Geos Model Devel 9(4):1567-1596. https://doi.org/10.5194/gmd-9-1567-2016

Grelle G, Wood C, Bonito L, et al. (2018) A reliable computerized litho-morphometric model for development of 3D maps of Topographic Aggravation Factor (TAF): the cases of East Mountain (Utah, USA) and Port au Prince (Haiti). Bul Earth Eng 16(5):1725-1750. https://doi.org/10.1007/s10518-017-0272-x

Grelle G, Gargini E, Facciorusso J, et al. (2020) Seismic site effects in the Red Zone of Amatrice hill detected via the mutual sustainment of experimental and computational approaches. Bul Earth Eng 18(5):1955-1984. https://doi.org/10.1007/s10518-019-00777-z

Grelle G, Bonito L, Rosalba M, et al. (2020) Topographic effects observed at Amatrice hill during the 2016-2017 Central Italy seismic sequence. Earth Eng Eng Vibr 20 (1): 63-78. https://doi.org/10.1007/s11803-021-2005-z

Huang R, Li W (2008) Research on development and distribution rules of geohazards induced by Wenchuan earthquake on 12th May, 2008. Chin J Rock Mech Eng 27(12):2585-2592. (In Chinese). https://doi.org/10.3321/j.issn:1000-6915.2008.12. 028

Huang S, Lv Y, Peng Y (2016) Dynamic response of sandy slope under coupling of earthquake and groundwater. Geotech Geol Eng 34(3): 889-899. https://doi.org/10.1007/s10706-016-0014-x

Hough SE, Altidor JR, AngladeD, et al. (2010) Localized damage caused by topographic amplification during the 2010 M 7.0 Haiti earthquake. Nat Geosci 3(11): 778-782. https://doi.org/10.1038/ngeo988

Jafarzadeh F, Shahrabi MM, Jahromi HF (2015) On the role of topographic amplification in seismic slope instabilities. J Rock Mech Geo Eng 7(2):163-170. https://doi.org/10.1016/j.jrmge.2015.02.009

Luo Y, Lei W, Wang Y, et al. (2021) Revealing the geological materials properties by a shallow seismic method for investigating slope site effects: a case study of Qiaozhuang town, Qingchuan County, China. Arab J Geosci 14(2):1-15. https://doi.org/10.1007/s12517-020-06379-3

Luo Y, Fan X, Huang R, et al. (2020) Topographic and near-surface stratigraphic amplification of the seismic response of a mountain slope revealed by field monitoring and numerical simulations. Eng Geol 271:105607. https://doi.org/10.1016/j.enggeo.2020.105607

Luo Y, Del Gaudio V, Huang R, et al. (2014) Evidence of hillslope directional amplification from accelerometer recordings at Qiaozhuang (Sichuan—China). Eng Geo 183: 193-207. https://doi.org/10.1016/j.enggeo.2014.10.015

Lawrence LD, Lewis RW(1973) Observed effects of topography on ground motion. Bull Seismo Soc Am 63 (1): 283-298. https://doi.org/10.1785/BSSA0630010283

Liu G, Li Y, Chen J(2009) The Problem of Earthquake Fault about Qiaozhuang Town in the Qingchuan County after Wenchuan Earthquake. J Mt Sci 4: 017. (In Chinese). https://doi.org/10.1042/BSR20080061

Maufroy E, Cruz A, Cotton VM, et al. (2015) Frequency-scaled curvature as a proxy for topographic site‐effect amplification and ground‐motion variability. Bull Seismol Soc Am 105(1): 354-367.https://doi.org/10.1785/0120140089

Maufroy E, Cruz A, Gafet S (2012) A robust method for assessing 3-D topographic site efects: a case study at the LSBB underground laboratory. Earth Spectra 28(3):1097-1115. https://doi.org/10.1193/1.4000050

Martino S, Minutolo A, Paciello A, et al. (2006) Evidence of amplification effects in fault zone related to rock mass jointing. Nat Hazards 39(3): 419-449. https://doi.org/10.1007/s11069-006-0001-2

Rai M, Rodriguez MA, Yong A (2016) An empirical model to predict topographic efects in strong ground motion using California small- to medium-magnitude. Earth Spectra 32(2):1033-1054. https://doi.org/10.1193/113014eqs202m

Semblat JF, Duval AM, Dangla P(2000) Numerical analysis of seismic wave amplification in Nice (France) and comparisons with experiments. Soil Dyn Earth Eng 19(5): 347-362. https://doi.org/10.1016/S0267-7261(00)00016-6

Scott AA, Nicholas S, John L, et al. (1997) Topographic effects on the seismic response of steep slopes. Bull Seismol Soc Am 87 (3): 701-709. https://doi.org/10.1029/96JB03485

Sepúlveda SA, Murphy W, Jibson RW, et al. (2005) Seismically induced rock slope failures resulting from topographic amplification of strong ground motions: The case of Pacoima Canyon, California. Eng Geo 80(3-4):336-348. https://doi.org/10.1016/j.enggeo.2005.07.004

Sheng J, Wang Z (2009) Emergency governance project investigation report of Weigan hill unstable slope in Qingchuan County of Sichuan Province. Geotechnical engineering emergency exploration report. pp 6-43 (In Chinese).

Tao Z, Tao X (2021)Discussion on the Grade scales of Natural Disasters by the loses in Wenchuan Earthquake. J Catast 36(4) : 31 -36(In Chinese). https://doi:10.3969/j.issn.1000 -811X.2021.04.006.

Torgoev A, Havenith HB (2016) 2D dynamic studies combined with the surface curvature analysis to predict Arias Intensity amplification. J Seismol 20(3): 711-731. https://doi.org/10.1007/s10950-016-9553-0

Wang G, Du C, Huang D, et al. (2018) Parametric models for 3D topographic amplification of ground motions considering subsurface soils. Soil Dyn Earth Eng 115:41-54. https://doi.org/10.1016/j.soildyn.2018.07.018

Wong HL, Jennings PC (1975) Effects of canyon topography on strong ground motion. Bull Seismol Soc Am 65(5):1239-1257. https://doi.org/10.1785/BSSA0650051239

Xu Q, Zhang Y, Feng W (2009a) Emergency governance project investigation report of Mt.Dong unstable slope in Qingchuan County of Sichuan Province. Geotechnical engineering emergency exploration report. pp 6-44. (In Chinese).

Xu Q, Zhang Y, Feng W (2009b) Emergency governance project investigation report of Mt.Shizi unstable slope in Qingchuan County of Sichuan Province. Geotechnical engineering emergency exploration report. pp 1-61. (In Chinese).

GB 50011-2010. Code for seismic design of buildings.China Construction Industry Press. pp 254-255. (In Chinese)